Chapter 4

Exploration of the genesis of whirlwinds: Application to dust devils

4.1 Introduction

Unlike huge sized mighty tornadoes and hurricanes, dust-devils are transient whirlwinds, rotating at a small scale, mixed with dust particles, dry leaves and anything else available in the surroundings lying on the ground and light enough to float in the air, observed particularly in the summer. A dust devil, also called a twister, is witnessed lasting even for several minutes but less frequently.

Out of the numerous scientific reports published for over a century, we shall discuss only those which give prime importance to the radial velocity with an intention to construct a model for dust-devils, more general than existing ones.

Burgers (1940, 1948) and Long-Rott (Long, 1957; Rott, 1958) independently modelled steady viscous vortex motion with a radially inward stagnation point flow over a plane boundary with the radial velocity, $u = -ar$, the axial velocity, $w = 2az$, and the azimuthal velocity, $v(r,t) = \frac{\Gamma_0}{2\pi r}\{1 - \exp(-\frac{ar^2}{2\nu})\}$, where $a = -(\partial u/\partial r)_0$. The model is referred to as Burgers-Rott vortex model.

Sullivan (1959) provided an exact solution for a two-celled vortex motion which despite some similarity with the Burgers-Rott one cell vortex model is more general than it. It has an inner cell in which air flow descends from above and flows outward to meet a separate air flow which converges radially. It is the simplest vortex that describes the flow in an intense tornado with a central downdraft which flows outward to join the circumferential updraft. The Sullivan vortex is given by $u = -ar + \frac{6\nu}{r}(1-\exp(-\frac{ar^2}{2\nu}))$, $w = 2az(1-3\exp(-\frac{ar^2}{2\nu})$ and $v = \frac{\Gamma}{2\Pi r}\frac{H(\frac{ar^2}{2\nu})}{H(\infty)}$, where Γ is the circulation strenght of the vortex, $a = -(\partial u/\partial r)_0$ is the strength of the suction and $H(x)$ is the function defined as $H(x) = \int_0^x \exp(f(t))$, where $f(t) = -t+3\int_0^t(1-\exp(-y))dy/y$. Here ν is considered to be a constant eddy viscosity which dominates the value of this coefficient, not molecular viscosity. The pressure distribution in the atmosphere is given by $p(r,z) = p_0 + \rho\int_0^r \frac{v^2}{r}dr - \frac{\rho r^2}{2}(r^2+4z^2) - \frac{18\rho v^2}{r^2}(1-\exp(-\frac{ar^2}{2\nu}))$ and the axial pressure gradient is $\partial p/\partial z = -4\rho z a^2$, which increases vertically in magnitude.

Vatistas (1986) experimentally observed that in the concentrated vortex, the azimuthal velocity component does not depend strongly on the axial coordinate. Therefore, under these assumptions the radial velocity component can be obtained from the θ-momentum equation, the normalised radial velocity function $\overline{u}$ is given by $\overline{u} = u\frac{r_c}{\nu} = -\{\frac{2(1+n)\bar{r}^{2n-1}}{(1+\bar{r}^{2n})}\}$, where ν is the kinematic viscosity and the normalized axial velocity function $\overline{V_z}$ is given by $\overline{w} = w\frac{r_c}{\nu} = \frac{4n(1+n)\bar{r}^{2n-1}}{(1+\bar{r}^{2n})^2}$. This approaches Rankine profile as $n \to \infty$. These equations have singularity on the vortex center

for $n < 1$. Therefore distribution with for $n < 1$ should not be permitted. For any finite value of n, the values of all velocity components are well behaved. The Vatistas (1991) generalised a few of the well-known vortex tangential velocity in aerodynamics.

Deissler (1977) dealt with different aspects of atmospheric vortices by considering a single gravity driven vortex and a frictionless adiabatic model. It was a generalisation of the model given by Deissler and Boldman (1974). The azimuthal velocity v is a function of only r, the radial coordinate, while the axial velocity w depends on only z, the axial coordinate. The radial velocity u is then computed and found to be dependent on r and z.

Several reports deal with tornado dynamics. Ward (1956) used a laboratory model to study temperature inversion as a factor in the formation of tornadoes. Kuo (1966) did an analytical study of the dynamics of convective atmospheric vortices. He (1967) later wrote a note on the similarity solutions of the vortex equations in an unsteady stratified atmosphere. Bellany-Knights (1970) got an unsteady two cell solution of the Navier–Stokes equations. Serrin (1972) modelled a swirling vortex in the spherical polar coordinates. He himself (1972) later explored certain features of tornado dynamics using a laboratory model. Lewellen (1993) detailed a comprehensive theory of tornado vortex. Larcheveque and Chaskalovic (1994) put forward a theory for tornado genesis and found that the basic flow is generated simultaneously by a strong vertical gradient of temperature and by a storm in the troposphere, which is a non-rotating updraft. The aforementioned literature gives due weightage to the radial velocity. Their generalisations have also been subsequently attempted. Davies-Jones (1995) discussed tornadoes extensively.

Anderson et al. (2006) modelled bath tub vortex in a rotating container and proposed a model with zero axial velocity $u = -F/\pi r\delta \times e^{-z/\delta} sin(z/\delta)$, $v =$

$F/\pi r\delta \times \left(1 - e^{-z/\delta}\right) cos(z/\delta)$ where F is the flow rate, δ is the Ekman layer thickness. The most recent reports are confined to different aspects particularly of tornado like vortices, and used different methods for solution. In all such communications, radial velocity has been given prime importance (Tanamachi et al., 2006; Yih, 2007; Makarieva and Gorshkov, 2009*a*, 2009*b*, 2011; Bestray et al., 2011; Makarieva et al., 2011; Arsen'yev, 2011; Bistray and Lykov, 2012; Rotunno, 2013; Davies-Jones, 2015; Ben-Amots, 2016; Baker and Sterling, 2017 etc.).

Although in a few of the models available in the literature, the axial velocity has not been given importance (Rankine, 1882; Anderson et al., 2006; Wood and White, 2011); but in several models, to be discussed hereinafter, it has been duly taken care of. While a few showed its dependence on either the axial coordinate (Burgers, 1948-Rott, 1959; Deissler, 1977) or the radial vector (Makarieva and Gorshkov, 2011; Pandey and Maurya, 2017), there are models in which the axial velocity depends on both (Sullivan, 1959). This is due to various considerations for simplifying the complex governing equations or due to the physical phenomenon under consideration. Gall (1982) considered radial velocity depending on the radial as well as the axial coordinates while analysing the internal dynamics of tornadoes and further derived the axial velocity which depends on both. Baker and Sterling (2017) considered a particular form of the radial velocity for inviscid flow and derived the axial velocity in terms of both the radial and the axial coordinates. A comparative study of analytical and empirical models has been presented by Kim and Matsui (2017). Gillmeier et al. (2018) have also reviewed analytical tornado-like vortex flow field models.

In a recent publication, Pandey and Maurya (2017), while exploring the characteristics of whirlwind, concluded that a low pressure zone is essentially required for any vortex motion for its survival. The model they presented possesses

axial and azimuthal velocities. The radial component was neglected justifying its insignificance in terms of magnitude in a mature whirlwind. However, the fact is that this is the first and foremost velocity and causes the birth of any such vortex motion despite the fact that later, other components of velocity become more significant and dominating.

The discussion throughout the introduction is confined to those papers which considered the significance of the radial component and eventually formulated it in the models they presented. Considering this aspect, we intend to incorporate the radial velocity in the model presented by Pandey and Maurya (2017) in order to examine its impact on the flow behaviour of dust devils. Accordingly, changes are expected in the axial and azimuthal components of velocity.

4.2 Mathematical formulation of the problem

We shall first discuss the physical model of the dust devil that is to be translated into a mathematical formulation which characterizes its motion for further solution and subsequent discussion.

4.2.1 The physical model

During the summer season, when a part of the Earth's surface is very much hot, a local low pressure region is created leaving the air rarer in density. It leads to a horizontal shear supplying the flow with vertical vorticity and a mild wind blows between $3 - 10$ *mph*. A twister is then created in planes and deserts due to super-adiabatic temperature lapse rate with an unstable temperature stratification (Barcilon, 1967). Ives (1947) reported that dust devils can be started by mild disturbances such as

firing of a shell in a mirage or running of a small animal across a mirage area in deserts. Horizontal breeze that causes radial velocity plays a big role in the formation of a dust devil. In a mature tornado, it may be insignificant; yet the centripetal acceleration is required to keep it rotating, which is due to the presence of a low pressure zone in the middle (Pandey and Maurya, 2017). However, even after a dust devil matures, the ambience around it keeps it disturbing and therefore presence of radial velocity cannot be ruled out.

Horizontally blowing mild breezes rush to the low pressure zone and are then diverted upward by the compressed air lying midway, adding momentum to rising hot air and making the dust devil visible by lifting dust, sand, debris, and leaves etc. which later float due to buoyancy and keep rotating with the twisting wind. Although the pressure inside the twister is low, that around it which is due to the winds coming from relatively cold places can be comparatively high. The density of these winds can be more in magnitude since these contain more humidity and carry dust, debris, leaves etc. Areas prone to dust devils are hot, flat surfaces such as dry playas and riverbeds (Mattsson et al., 1993), close to freshly ploughed and irrigated fields (Sinclair, 1969), gentle slopes (Brooks, 1960). The details are nicely given in a review paper of Balme and Greeley (2006). The observations divulge the fact that not the heat but it is the temperature gradient that creates favorable circumstances for the birth of whirlwinds. Rafkin et al. (2016) finds a convective vortex as the first criterion for the formation of dust devils, the other two being: sufficient strength of the associated winds to loft sand or the other particulates into the air, and a sufficient source of mobile surface material to produce visible opacity. However, low background winds' theory of McGinnigle (1966) and wind threshold finding of Sinclair (1969) still leave scope for a better fluid dynamic theory to come up.

Winds are certainly compressible but if these are not deliberately compressed, one may consider them incompressible for the sake of modelling. Of course, when the low pressure zone inside the twister gets gradually filled with cold wind with high pressure, it will die out. It is to be noted that thermodynamics has a great role to play and several authors take it into consideration, discuss and incorporate in their models (Larcheveque and Chaskalovic, 1994). However here, although we do not rule out its role but consider only its impact which ultimately affects pressure and velocity of the whirlwind. There are many more issues to be addressed here.

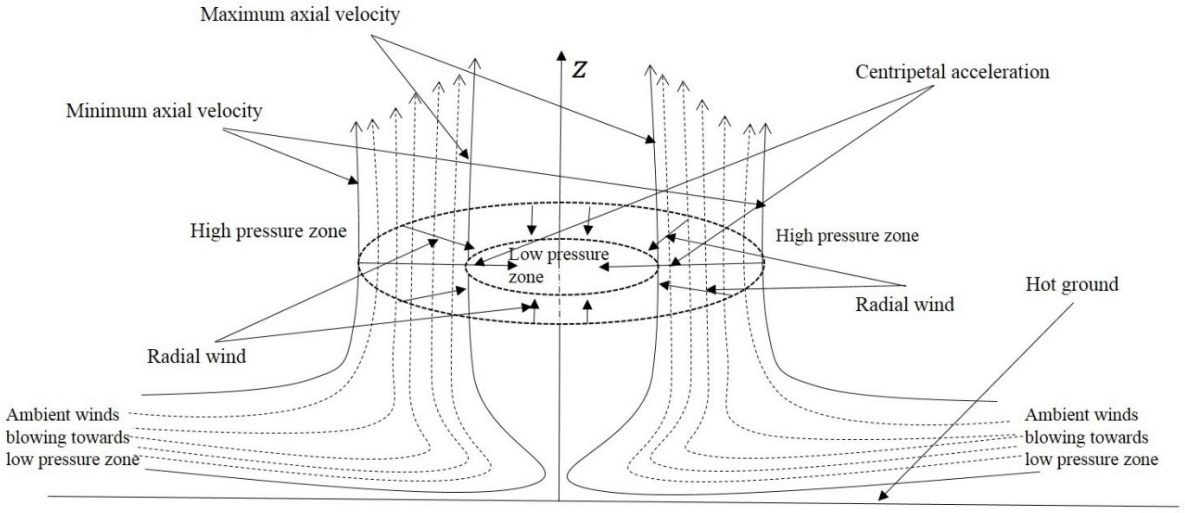

Figure 4.1: Schematic diagram of the formation of a whirlwind (dust-devils). Dashed curves show the direction of the ambient winds blowing horizontally and getting diverted upward by the compressed air lying in the buffer zone, the innermost and the outermost layers being shown by solid curves. Heights of the different layers indicate that the innermost layer rises the most. The two dotted circles indicate the inner and the outer boundaries of the rotating annular dust devil around a low pressure zone and kept intact by centripetal acceleration and the arrows between the annular regions indicate the direction of the inflow radial component of the wind.

4.2.2 Mathematical model of whirlwind vortex

In cylindrical polar coordinates (r, θ, z), r, θ, z respectively represent the radial, azimuthal and axial coordinates. Considering the whirlwind rotating symmetrically about the vertical axis, we remove all terms involving θ. Thus, the three-dimensional Navier-Stokes governing equations for the steady axi-symmetrically rotating flow of an incompressible Newtonian viscous fluid may be given by

$$\rho\left(u\frac{\partial u}{\partial r}+w\frac{\partial u}{\partial z}-\frac{v^2}{r}\right)=-\frac{\partial p}{\partial r}+\mu\left(\frac{\partial^2 u}{\partial r^2}+\frac{1}{r}\frac{\partial u}{\partial r}-\frac{u}{r^2}+\frac{\partial^2 u}{\partial z^2}\right), \tag{4.1}$$

$$\rho\left(u\frac{\partial v}{\partial r}+w\frac{\partial v}{\partial z}+\frac{uv}{r}\right)=\mu\left(\frac{\partial^2 v}{\partial r^2}+\frac{1}{r}\frac{\partial v}{\partial r}-\frac{v}{r^2}+\frac{\partial^2 v}{\partial z^2}\right), \tag{4.2}$$

$$\rho\left(u\frac{\partial w}{\partial r}+w\frac{\partial w}{\partial z}\right)=-\rho g\frac{\rho_\infty-\rho}{\rho_\infty}-\frac{\partial p}{\partial z}+\mu\left(\frac{\partial^2 w}{\partial r^2}+\frac{1}{r}\frac{\partial w}{\partial r}+\frac{\partial^2 w}{\partial z^2}\right), \tag{4.3}$$

together with the continuity equation

$$\frac{1}{r}\frac{\partial(ru)}{\partial r}+\frac{\partial w}{\partial z}=0. \tag{4.4}$$

where u, v and w denote the fluid motion respectively in the $r-$, $\theta-$ and $z-$ directions with p being the pressure, ρ the density and μ the viscosity of the fluid, and ρ and ρ_∞ respectively the densities of the fluid contained in the dust devil and that of the ambient wind. Besides, $g = G\frac{M}{(R+h(z))^2}$ is the gravitational acceleration G, M, R, h, being respectively the Gravitational constant, the mass of the earth, the radius of the earth and the height which is a function of z. g, may be taken as a constant in view of $h(z)$ being negligibly small in comparison to R. The modified gravitational acceleration term in Eq. (4.3) is based on Simpson and Glezer (2016).

We consider a whirlwind more general than that considered by Pandey and Maurya (2017). Though the model is more general, the fluid assumed is still

Newtonian and incompressible. To begin with, Pandey and Maurya (2017) assumed the azimuthal velocity of a particular form and the radial velocity negligibly small. With these assumptions, they derived the axial velocity as a function of only r. However, some of the researchers, as discussed in the introduction, assumed the radial velocity non-zero and a function of r for some axially rotating vortex like motions applicable to the natural phenomena such tornadoes, typhoons, hurricanes, cyclones etc. Thus, it may be generalised as $u(r)$.

We proceed with the physical model of whirlwind as considered by Pandey and Maurya (2017) with the exception that the radial velocity is not negligible and hence retained and that the axial velocity is dependent on the radial coordinate. Thus, the whirlwind, a vertical circularly rotating fluid mass, is modelled as a cylindrical annulus of dense areal mass, inside which is a rarer areal mass region, which creates a favourable radial gradient of pressure. Hence, there are two concentric vertical cylindrical surfaces, say innermost and outermost surfaces. The annular mass rotates with varying azimuthal velocities. Let the innermost one, which is in contact with low pressure region, rotate with the highest axial velocity, vertically upward being the positive direction. The concentric layers slow down as we move towards the outermost surface and the axial velocity of the outermost layer may be asymptotically zero in some cases.

With the aforementioned consideration of the axial velocity $w(r, z)$ and the radial velocity $u(r)$ for steady flow, the governing Eqs. (4.1−4.4) reduce to

$$\frac{du}{dr} - \frac{v^2}{r} = -\frac{1}{\rho}\frac{\partial p}{\partial r} + \nu\left(\frac{d^2u}{dr^2} + \frac{1}{r}\frac{du}{dr} - \frac{u}{r^2}\right), \tag{4.5}$$

$$u\left(\frac{\partial v}{\partial r} + \frac{v}{r}\right) + w\frac{\partial v}{\partial z} = \nu\left(\frac{\partial^2 v}{\partial r^2} + \frac{1}{r}\frac{\partial v}{\partial r} - \frac{v}{r^2} + \frac{\partial^2 v}{\partial z^2}\right), \tag{4.6}$$

$$u\frac{\partial w}{\partial r} + w\frac{\partial w}{\partial z} = -g\frac{\rho_\infty - \rho}{\rho_\infty} - \frac{1}{\rho}\frac{\partial p}{\partial z} + \nu\left(\frac{\partial^2 w}{\partial r^2} + \frac{1}{r}\frac{\partial w}{\partial r} + \frac{\partial^2 w}{\partial z^2}\right), \tag{4.7}$$

$$\frac{1}{r}\frac{d(ru)}{dr} + \frac{\partial w}{\partial z} = 0. \tag{4.8}$$

4.2.3 Estimation of radial velocity

We use the method of separable variables for $w(r, z)$ for solution and under the assumptions that the radial velocity u is a function of only r and the axial pressure gradient $\partial p/\partial z$ is a constant, we arrive at the conclusion that w is a function of only r. The details are given in **Appendix A**. In view of that analysis and conclusion, Eq. (4.7) reduces to

$$u\frac{dw}{dr} = -g\frac{\rho_\infty - \rho}{\rho_\infty} - \frac{1}{\rho}\frac{\partial p}{\partial z} + \nu\left(\frac{d^2 w}{dr^2} + \frac{1}{r}\frac{dw}{dr}\right), \tag{4.9}$$

Further, from the continuity Eq. (4.8), we obtain the radial velocity

$$u(r) = -\frac{c}{r}, \tag{4.10}$$

where c is an arbitrary constant. For the arguments given in the Section 4.2.5 discussing azimuthal velocity (given by Eq. (4.15)), it is appropriate to consider $u(r)$ negative and thus c is positive presented with a minus sign. Let us name c inflow-parameter. Unlike Burgers-Rott vortex model in which the radial velocity $u \propto r$, this form is somewhat similar to the radial velocity given by Andersen et al. (2006) for a bathtub in which $u \propto 1/r$.

4.2.4 Estimation of axial velocity

Now we solve Eq. (4.9) for axial velocity under the assumption that the axial velocity is maximum at the innermost radius r_i and is minimum w_0 (maybe even zero) at its outermost layer r_o. Thus, the axial velocity may be given by

$$w(r) = w_0 - \frac{g\frac{\rho_\infty - \rho}{\rho_\infty} + P}{\rho\nu}\left[\frac{r_i^{2+c/\nu}\left(r_o^{-c/\nu} - r^{-c/\nu}\right)}{c/\nu\,(2+c/\nu)} + \frac{r_o^2 - r^2}{2\,(2+c/\nu)}\right] \tag{4.11}$$

where P, symbolising $\partial p/\partial z$, is constant. When $c \to 0$, as a limiting case, Eq. (4.11) for the axial velocity $w(r)$ reduces to that derived by Pandey and Maurya (2017) for $u(r) \to 0$.

4.2.5 Estimation of azimuthal velocity

Considering the azimuthal velocity a function of only r (as per the conclusion given in Appendix C), i.e., $v = v(r)$, Eq. (4.6) reduces to

$$-\frac{c}{r}\left(\frac{dv}{dr} + \frac{v}{r}\right) = \nu\left(\frac{d^2v}{dr^2} + \frac{1}{r}\frac{dv}{\partial r} - \frac{v}{r^2}\right), \tag{4.12}$$

Rearranging of Eq. (4.12) reduces it to Cauchy-Euler type ordinary differential equation

$$r^2\frac{d^2v}{dr^2} + r\left(1 + \frac{c}{\nu}\right) - \left(1 - \frac{c}{\nu}\right)v = 0, \tag{4.13}$$

giving the solution

$$v(r) = \frac{A}{r} + Br^{1-c/\nu}, \tag{4.14}$$

where A and B are integration constants.

Using boundary conditions that the innermost layer is moving with the uniform angular velocity ω_i and the outermost layer with ω_o, we obtain the azimuthal velocity

$$v(r) = \frac{1}{r_o^{2-c/\nu} - r_i^{2-c/\nu}} \left[r^{1-c/\nu} \left(r_o^2 \omega_o - r_i^2 \omega_i \right) - \frac{r_i^{2-c/\nu} r_o^{2-c/\nu} \left(\omega_o r_o^{c/\nu} - \omega_i r_i^{c/\nu} \right)}{r} \right], \tag{4.15}$$

For negligibly small radial velocity,

$$v(r) \to \frac{1}{r_o^2 - r_i^2} \left[\left(r_o^2 \omega_o - r_i^2 \omega_i \right) r - \frac{r_i^2 r_o^2 \left(\omega_o - \omega_i \right)}{r} \right], as, c \to 0$$

which was derived by Pandey and Maurya (2017) for a whirlwind without radial velocity. Further, when the radius r with $r_i \leq r \leq r_o$, of the whirlwind increases infinitely, the azimuthal velocity reduces to zero, i.e., $v(r) \to$ as $r \to \infty$.

4.2.6 Vorticity vector

Thus, in the consolidated form, the velocity of the vortex may be given by

$$\left.\begin{aligned} u(r) &= -\frac{c}{r}, \\ v(r) &= \frac{1}{r_o^{2-c/\nu} - r_i^{2-c/\nu}} \left[r^{1-c/\nu} \left(r_o^2 \omega_o - r_i^2 \omega_i \right) - \frac{r_i^{2-c/\nu} r_o^{2-c/\nu} \left(\omega_o r_o^{c/\nu} - \omega_i r_i^{c/\nu} \right)}{r} \right], \\ w(r) &= w_0 - \frac{g\frac{\rho_\infty - \rho}{\rho_\infty} + P}{\rho\nu} \left[\frac{r_i^{2+c/\nu} \left(r_o^{-c/\nu} - r^{-c/\nu} \right)}{c/\nu \left(2 + c/\nu \right)} + \frac{r_o^2 - r^2}{2 \left(2 + c/\nu \right)} \right]. \end{aligned}\right\}$$

Hence, the corresponding vorticity vector is given by

$$\boldsymbol{\zeta} = \hat{\boldsymbol{r}} 0 + \hat{\boldsymbol{\theta}} \frac{g\frac{\rho_\infty - \rho}{\rho_\infty} + P}{(2 + c/\nu)\mu} \left(\frac{r_i^{(2+c/\nu)}}{r^{(1+c/\nu)}} - r \right) + \hat{\boldsymbol{z}} \frac{-(2 - c/\nu)(r_i^2 \omega_i - r_o^2 \omega_o) r^{-c/\nu}}{r_o^{2-c/\nu} - r_i^{2-c/\nu}},$$

which, for negligible radial velocity (i.e. $c \to 0$), reduces to

$$\boldsymbol{\zeta} = \hat{\boldsymbol{r}}0 + \hat{\boldsymbol{\theta}}\frac{g\frac{\rho_\infty - \rho}{\rho_\infty} + P}{2\mu}\left(\frac{r_i^2}{r} - r\right) + \hat{\boldsymbol{z}}\frac{-2(r_i^2\omega_i - r_o^2\omega_o)}{r_o^2 - r_i^2}, as, c \to 0.$$

4.2.7 Radial pressure gradient

When we substitute $u(r)$ from Eq. (4.10) into Eq. (4.5), we find that the entire viscous term vanishes and the radial pressure gradient reduce to

$$\frac{\partial p}{\partial r} = \rho\left(\frac{c^3}{r^3} + \frac{v^2}{r}\right), \tag{4.16}$$

which, with the azimuthal velocity substituted from Eq. (4.15), may be given by

$$\frac{\partial p}{\partial r} = \rho\left[\frac{c^3}{r^3} + \frac{1}{r}\left\{\frac{r_i^2 r_o^2\left(r_o^{-c/\nu}\omega_i - r_i^{-c/\nu}\omega_o\right)}{r_o^{2-c/\nu} - r_i^{2-c/\nu}}\frac{1}{r} + \frac{\left(r_o^2\omega_o - r_i^2\omega_i\right)r^{1-c/\nu}}{r_o^{2-c/\nu} - r_i^{2-c/\nu}}\right\}^2\right], \tag{4.17}$$

Integrating Eq. (4.17) from r_i to r, we get

$$\begin{aligned} p(r,z) - p(r_i,z) = \frac{\rho}{2}\Bigg[&\left\{c^2 + \left(\frac{r_i^2 r_o^2\left(r_o^{-c/\nu}\omega_i - r_i^{-c/\nu}\omega_o\right)}{r_o^{2-c/\nu} - r_i^{2-c/\nu}}\right)^2\right\}\left(\frac{1}{r_i^2} - \frac{1}{r^2}\right) + \\ &\left(\frac{r_o^2\omega_o - r_i^2\omega_i}{r_o^{2-c/\nu} - r_i^{2-c/\nu}}\right)^2 \times \frac{r^{2(1-c/\nu)} - r_i^{2(1-c/\nu)}}{(1-c/\nu)} - \\ &\frac{4r_i^2 r_o^2\left(r_o^{-c/\nu}\omega_i - r_i^{-c/\nu}\omega_o\right)\left(r_o^2\omega_o - r_i^2\omega_i\right)\left(r^{-c/\nu} - r_i^{-c/\nu}\right)}{c/\nu\left(r_o^{2-c/\nu} - r_i^{2-c/\nu}\right)^2}\Bigg], \end{aligned} \tag{4.18}$$

In Eq. (4.11), the axial pressure gradient $\partial p/\partial z$ was considered a constant P. From there, we get

$$p(r,z) = p(r,z_0) + P(z - z_0), \tag{4.19}$$

where z_0 is reference point in the axis (see the details in **Appendix B**). Evaluating $p(r,z)$ for $r = r_i$ from Eq. (4.19) and then substituting $p(r_i,z)$ into Eq. (4.18), we obtain

$$p(r,z) - p(r_i,z_o) = (z-z_0)P + \frac{\rho}{2}\left[\left\{c^2 + \left(\frac{r_i^2 r_o^2\left(r_o^{-c/\nu}\omega_i - r_i^{-c/\nu}\omega_o\right)}{r_o^{2-c/\nu} - r_i^{2-c/\nu}}\right)^2\right\}\left(\frac{1}{r_i^2} - \frac{1}{r^2}\right) + \left(\frac{r_o^2\omega_o - r_i^2\omega_i}{r_o^{2-c/\nu} - r_i^{2-c/\nu}}\right)^2 \times \frac{r^{2(1-c/\nu)} - r_i^{2(1-c/\nu)}}{(1-c/\nu)} - \frac{4r_i^2 r_o^2\left(r_o^{-c/\nu}\omega_i - r_i^{-c/\nu}\omega_o\right)\left(r_o^2\omega_o - r_i^2\omega_i\right)\left(r^{-c/\nu} - r_i^{-c/\nu}\right)}{c/\nu\left(r_o^{2-c/\nu} - r_i^{2-c/\nu}\right)^2}\right], \tag{4.20}$$

In the limiting case, $\frac{r^{2(1-c/\nu)} - r_i^{2(1-c/\nu)}}{2(1-c/\nu)} \to log_e(\frac{r}{r_i})$, as, $c \to \nu$. Hence, for $c \to \nu$,

$$p(r,z) - p(r_i,z_o) = (z-z_0)P + \frac{\rho}{2}\left[\left\{c^2 + \frac{r_i^2 r_o^2\left(r_o\omega_o - r_i\omega_i\right)^2}{\left(r_o - r_i\right)^2}\right\}\left(\frac{1}{r_i^2} - \frac{1}{r^2}\right) + \frac{r_o^2\omega_o - r_i^2\omega_i}{\left(r_o - r_i\right)^2} \times \left\{2\left(r_i^2\omega_i - r_o^2\omega_o\right) log_e\left(\frac{r}{r_i}\right) - 4r_o r_i\left(r_o\omega_o - r_i\omega_i\right)\left(\frac{1}{r} - \frac{1}{r_i}\right)\right\}\right], \tag{4.21}$$

which is the same as that obtained when $c/\nu = 1$ is directly substituted in Eq. (4.13) and obtained from Eq. (4.16). Hence, the function is continuous at $c/\nu = 1$.

4.2.8 Streamlines and path lines

Equations for the streamlines and path lines can be seen in **Appendix D**.

4.3 Results and discussion

4.3.1 Radial velocity

Radial velocity is the genesis of vortex motion. Considering non-zero radial velocity and constant axial pressure gradient, we obtained $u(r) = -c/r$ from the continuity equation and the axial velocity $w(r)$, given by Eq. (4.11), was inferred as a function of r but not z. In the limiting case of zero radial velocity, it reduces to what Pandey and Maurya (2017) derived for a mature whirlwind. The azimuthal velocity $v(r)$, given by Eq. (4.15), was later deduced from Eq. (4.6). This reduces, as $c \to 0$, to the corresponding formulation of Pandey and Maurya (2017) for the model considering zero radial velocity.

Negative sign in the radial velocity $u(r) = -c/r$ is an indication that it is directed towards the centre, i.e., the axis of the whirlwind. The presence of an arbitrary constant suggests that although there is a pattern but it is not independent of other parameters. It is born naturally with a velocity depending upon the temperature of the surroundings. The nature shows that the radial velocity increases as it approaches the axis but practically it cannot reach the axis. We plot diagrams for arbitrary c shown in Fig. 4.2. We set the outermost radius $r_o = 1\ m$, $r_i = 0.1\ m$ and let r vary in the range $0.1\ m - 1.0\ m$. The arbitrary constant c is dimensionally similar to kinematic viscosity. Hence, it is assigned values comparative to the kinematic viscosity observed practically.

It is observed that the magnitude of the radial velocity increases as it moves towards the axis of the whirlwind. It obviously increases with the value of the parameter c (Fig. 4.2).

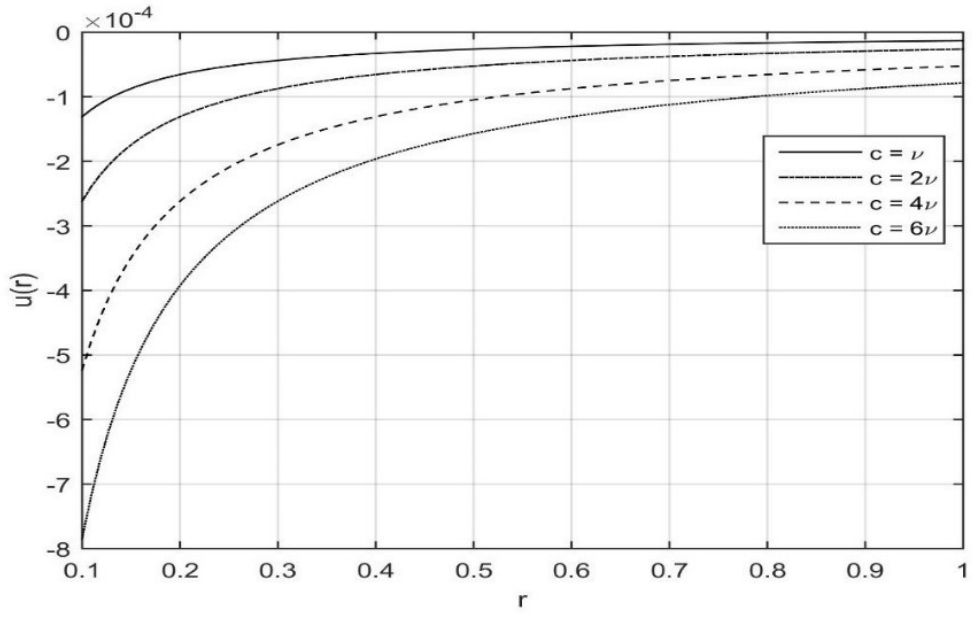

Figure 4.2: The diagram shows the radial velocity $u(r)$ distribution along the radail direction for various values of c based on Eq. (4.10).

4.3.2 Azimuthal velocity

The azimuthal velocity $v(r)$, given by Eq. (4.15), is dependent on the radial velocity and hence on c. Another important factor that determines the azimuthal velocity is ν, the kinematic viscosity. In Eq. (4.15), ν is present together with c, an arbitrary constant which is dimensionally similar to ν. For that reason, we draw plots for $v(r)$ vs. r corresponding to different values of c/ν by assigning fixed values for the innermost and the outermost radii. The plots are shown in Fig. 4.3. It is observed that $v(r)$ shoots up very close to the innermost radius for large values of c/ν but then gradually slows down to the velocity prescribed at the outer boundary. However, for no radial velocity, i.e., $c/\nu = 0$, $v(r)$ goes down right from the beginning.

The role of rotational motion is best interpreted by angular velocity. That is why, we deduce angular velocity from the azimuthal velocity and get

$$\omega\left(r\right)=\frac{1}{r_o^{2-c/\nu}-r_i^{2-c/\nu}}\left\{r^{-c/\nu}\left(r_o^2\omega_o-r_i^2\omega_i\right)-\frac{\omega_o r_i^{2-c/\nu}r_o^2-\omega_i r_i^2 r_o^{2-c/\nu}}{r^2}\right\} \tag{4.22}$$

In case, the innermost radius $r_i = 0$, the angular velocity appears to reduce to a very simple form, given by $\omega(r) = \omega_o \left(r_o/r\right)^{c/\nu}$. However, it is clear from the expression that $r \nrightarrow 0$. Thus $r_i \nrightarrow 0$. Further, we find that due to the presence of non-zero innermost radius in the denominator.

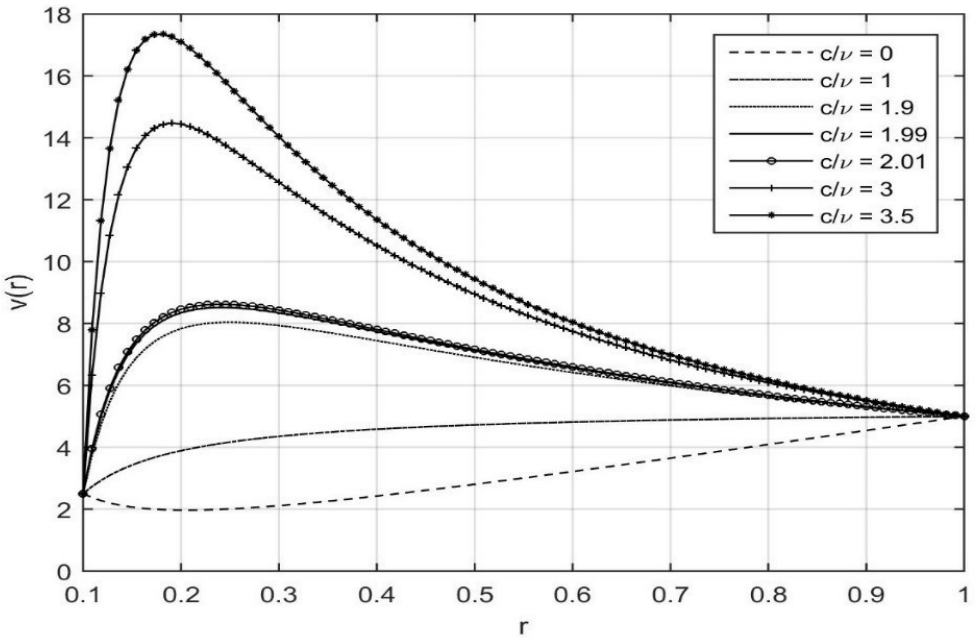

Figure 4.3: The diagram based on Eq. (4.15) shows the azimuthal velocity $v(r)$ distribution along the radial coordinate r for various values of the ratio c/ν. The velocity curve, corresponding to $c/\nu = 0$, describes the case for zero radial velocity. Other parameters are $\omega_i = 25\ cycles\ s^{-1}$ and $\omega_o = 5\ cycles\ s^{-1}$.

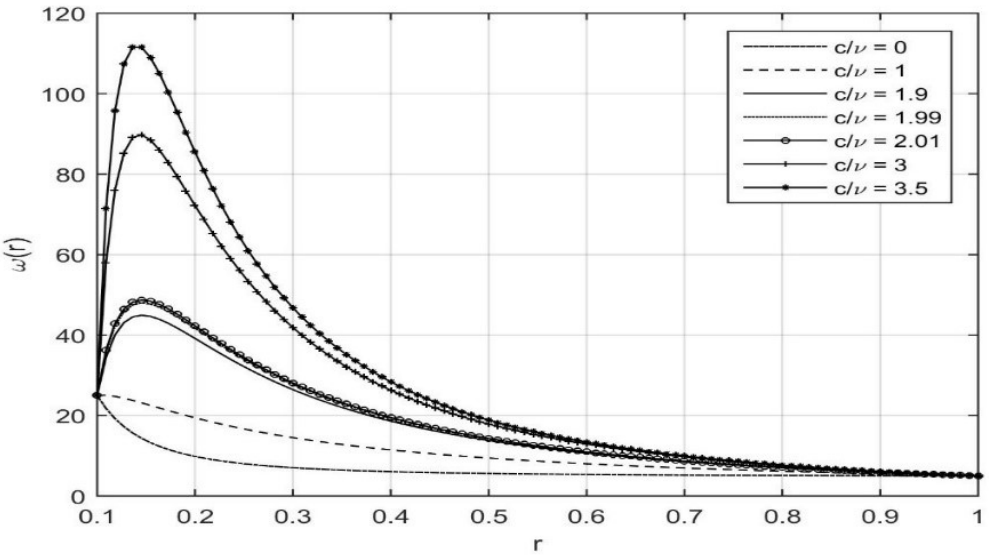

Figure 4.4: The diagram shows the angular velocity $\omega(r)$ distribution along the radial coordinate r for various values of the ratio c/ν. Other parameters are $\omega_i = 25\ cycles\ s^{-1}$ and $\omega_o = 5\ cycles\ s^{-1}$.

$$\omega\left(r\right) \rightarrow \frac{\omega_o r_o^2 log_e\left(\frac{r_i}{r}\right) - \omega_i r_i^2 log_e\left(\frac{r}{r_o}\right)}{r^2 log_e\left(\frac{r_i}{r_o}\right)}, as, c = 2\nu, \tag{4.23}$$

which is the same as that obtained by direct substitution $c = 2\nu$ in Eq. (4.13). This confirms continuity of the function at $c = 2\nu$.

We plotted graphs, by prescribing ω_i and ω_o for values of $c/\nu \in [0, 3.5]$ including 2 and close to 2 such as 1.99 and 2.01 shown in Fig. 4.4. It is observed that $\omega(r)$ touches its peak close to the innermost radius for large values of c/ν, but not at the innermost radius. For very small values of c/ν, it is not like that.

4.3.3 Axial velocity

The axial velocity $w(r)$ given by Eq. (4.11) is plotted against the radial coordinate (Fig. 4.5). It is observed that $w(r)$ has parabolic profile and the plots are similar to

what Pandey and Maurya (2017) observed for zero radial velocity despite the fact that Eq. (4.11) does not have logarithmic terms. We have already discussed that in the limiting case of $c \to 0$, we obtain $u(r) \to 0$ and the axial velocity $w(r)$ takes the form deduced by Pandey and Maurya (2017).

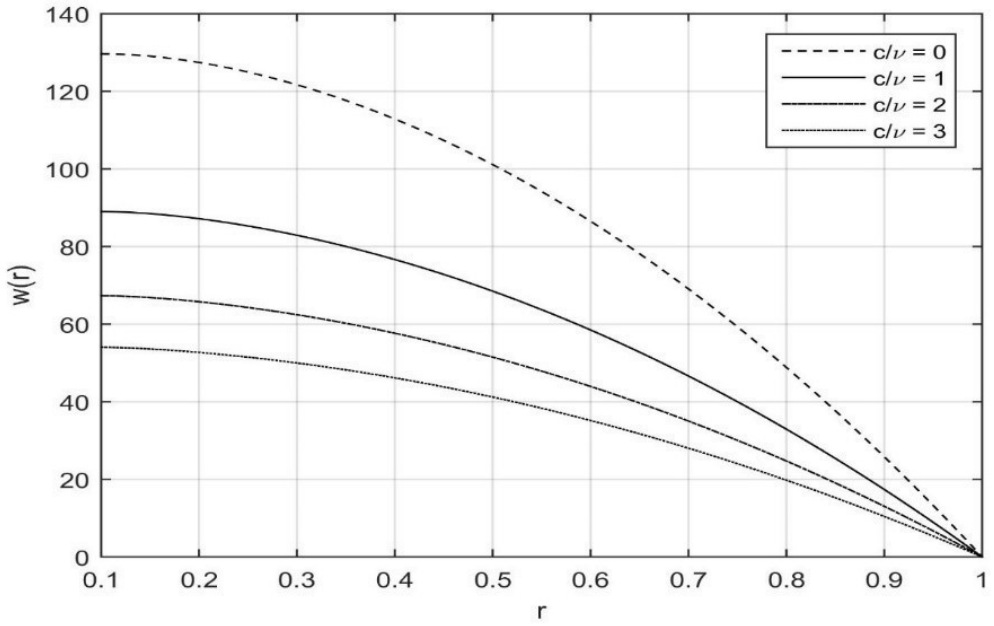

Figure 4.5: The diagram shows the axial velocity $w(r)$ distribution along the radial coordinate r for various values of the ratio c/ν based on Eq. (4.11). Other parameters used here are: dynamic viscosity $\mu(= \rho\nu) = 0.0000198\ Pa.s.$, $P = -0.01\ Pa/m$ and $w_o = 0$. The presence of g will simply reduce the magnitude slightly without disturbing the trends; hence it has not been under consideration.

4.3.4 Pressure

Pressure vs. radius plots exhibit an extraordinary behavior at $c = 2\nu$ (Figs. 4.6–4.10). Pressure function given by Eq. (4.20) is, however, continuous at $c = \nu$ as verified earlier and shows no anomalies (Figs. 4.6–4.7). For this reason, pressure curves corresponding to the values other than $c = 2\nu$ are shown in Fig. 4.6. The outermost radius is fixed as $r_o = 1.0\ m$ and the innermost radius r_i is varied in the range

$0.2\ m - 0.7\ m$. The value of c/ν is varied in the range $0.5 - 2.5$ excluding $c/\nu = 2$. Pressure is observed to rise from the innermost to the outermost radii. Pressure rises also with c/ν within some range of r_i (see Figs. 4.6$(a) - (b)$) and drops beyond that (see Fig. 4.6(c)).

In order to sort out this anomaly, we plot pressure against radius for different innermost radii r_i varying in the range $0.2\ m - 0.7\ m$ (Fig. 4.7) and different values of c/ν varying in the range $0.5 - 2.5$ with $r = 0.8\ m$, $0.9\ m$ fixed in two parts (a) and (b) of Fig. 4.7. For smaller values of r_i, pressure rises with c/ν but there is a turning point in the value of r_i beyond which the trend reverses. Interestingly, the turning point remains the same even when r changes. This is to be noted that the case $c/\nu = 2$ could not be considered as the corresponding values are quite large and was left for to be considered separately.

Treatment of the extraordinary case $c = 2\nu$

Let us examine the case $c = 2\nu$. In the limiting case,

$$\begin{aligned} p(r,z) - p(r_i,z) = (z - z_0)P + \frac{\rho}{2log_e^2\left(\frac{r_i}{r_o}\right)}\left(\frac{1}{r_i^2}\right. \\ \left. - \frac{1}{r^2}\right)\left[\left\{4\nu^2 log_e^2\left(\frac{r_i}{r_o}\right) + \left(\omega_o r_o^2 log_e(r_i) - \omega_i r_i^2 log_e(r_o)\right)^2\right\}\right. \\ + \left(\omega_i r_i^2 - \omega_o r_o^2\right) log_e\left(\frac{r}{r_i}\right)\left\{\omega_i r_i^2\left(1 - 4log_e(r_o) + log_e(rr_i)\right)\right. \\ \left.\left. - \omega_o r_o^2\left(1 - 4log_e(r_i) + log_e(rr_i)\right)\right\}\right],\ as,\ c \\ \rightarrow 2\nu, \end{aligned} \tag{4.24}$$

which is the same as the expression obtained by direct substitutions (i) $c/\nu = 2$ and (ii) $\omega(r)$ corresponding to $c/\nu = 2$ from Eq. (4.23), into Eq. (4.16).

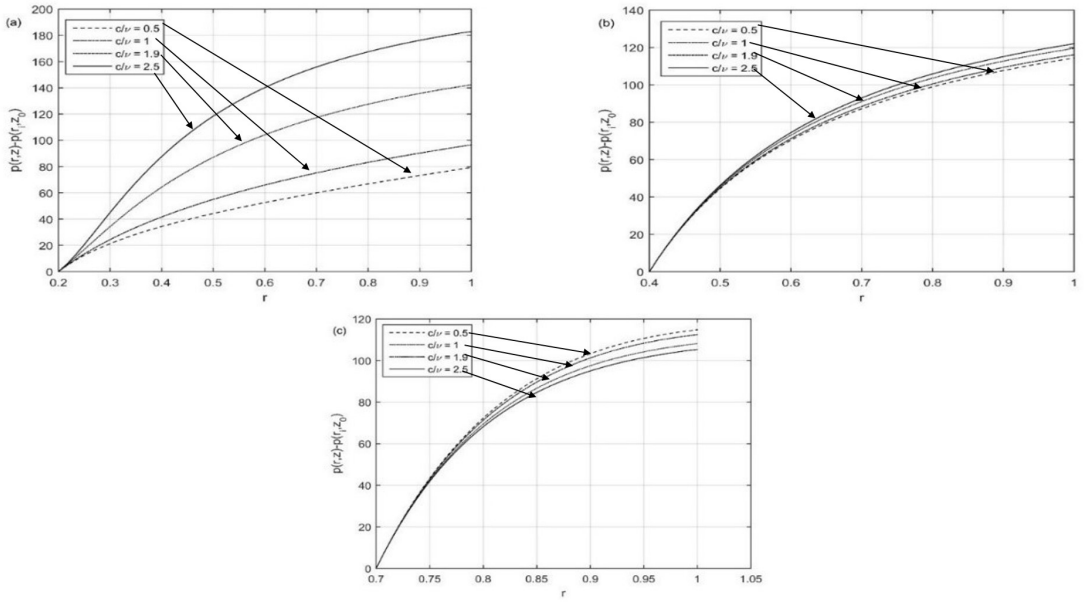

Figure 4.6: Diagrams based on Eq. (4.20) show the pressure $p(r,z) - p(r_i, z_o)$ distribution along the radial coordinate r for various values of the ratio c/ν. Other parameters set for the graphs are $\omega_i = 25\ cycles\ s^{-1}$, $\omega_o = 5\ cycles\ s^{-1}$, $r_o = 1.0\ m$ and $(a)\ r_i = 0.2\ m$, $r = 0.2\ m - 1.0\ m$, $(b)\ r_i = 0.4\ m$, $r = 0.4\ m - 1.0\ m$, $(c)\ r_i = 0.7\ m$, $r = 0.7\ m - 1.0\ m$.

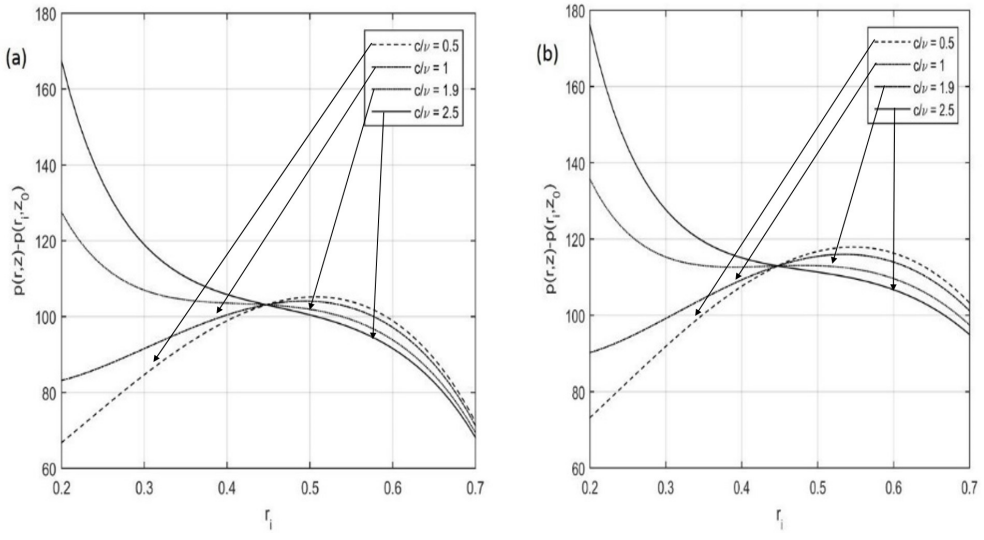

Figure 4.7: Diagrams based on Eq. (4.20) show the pressure $p(r,z) - p(r_i, z_o)$ at the radial coordinates $r = 0.8\ m$, $0.9\ m$ given in (a) and (b) parts of the figure respectively when r_i varies from $0.2\ m - 0.7\ m$ corresponding to various values of the ratio c/ν in the range $0.5 - 2.5$. Other parameters are $\omega_i = 25\ cycles\ s^{-1}$ and $\omega_o = 5\ cycles\ s^{-1}$.

In order to study variation of pressure in the neighbourhood of $c/\nu = 2$, we plot pressure against c/ν in the interval $[1.9999, 2.0001]$ by setting $r_i = 0.4\ m, 0.7\ m$, $r_o = 1.0\ m$ and $r \in [0.6, 0.9]\ m$ (Figs. 4.8$(a)-(b)$, 4.9$(a)-(b)$). Pressure is observed to rise at a tremendous rate to ultimately reach the pressure corresponding to $c/\nu = 2$. Still there is no discontinuity. The non-smoothness in the pressure graph is negligibly small and is due to the limitations of the software plotting graphs for extremely small variations. Fig. 4.10 shows the radial distribution of pressure corresponding to $c/\nu = 2$. If we compare Figs. 4.6(b) and 4.8(a) with Fig. 4.10, we find that the pressures corresponding to $r_o = 1.0\ m$, $r_i = 0.4\ m$, $r = 0.6\ m$ and $c/\nu = 2$ match in the those figures.

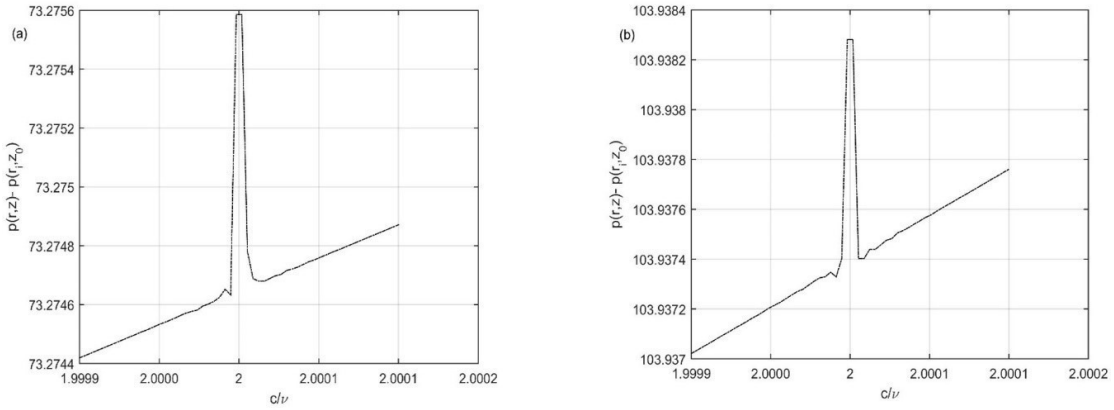

Figure 4.8: Diagrams based on Eq. (4.20) display plots for $p(r, z) - p(r_i, z_o)$ vs. c/ν. The various parameters are $r_o = 1.0\ m$, $r_i = 0.4\ m$ and $r = 0.6\ m, 0.8\ m$ respectively in (a) and (b). Other parameters are $\omega_i = 25\ cycles\ s^{-1}$ and $\omega_o = 5\ cycles\ s^{-1}$.

This extraordinary behaviour in a small neighbourhood of $c/\nu = 2$ adds a new dimension for investigation and physical interpretation.

The value of c/ν depends on a number of factors, e.g. c, μ and ρ, which are further dependent on pressure, temperature etc. Undoubtedly, these are unsteady in nature. It is quite natural that this is momentary and changes soon. Whenever we view a dust devil, we find that its start is sudden and fast and also that sometimes

during its course it enhances rotation by many folds by reducing its width. Hence, a momentary shock is predicted. Such shocks are often observed practically whenever a dust devil is born.

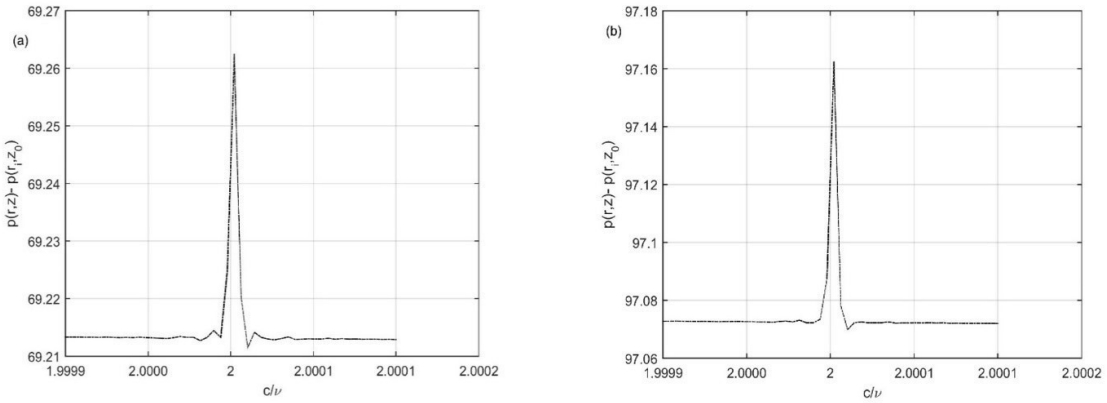

Figure 4.9: Diagrams based on Eq. (4.20) display plots for $p(r,z) - p(r_i, z_o)$ vs. c/ν. The various parameters are $r_o = 1.0\ m$, $r_i = 0.7\ m$ and $r = 0.8\ m, 0.9\ m$ respectively in (a) and (b). Other parameters are $\omega_i = 25\ cycles\ s^{-1}$ and $\omega_o = 5\ cycles\ s^{-1}$.

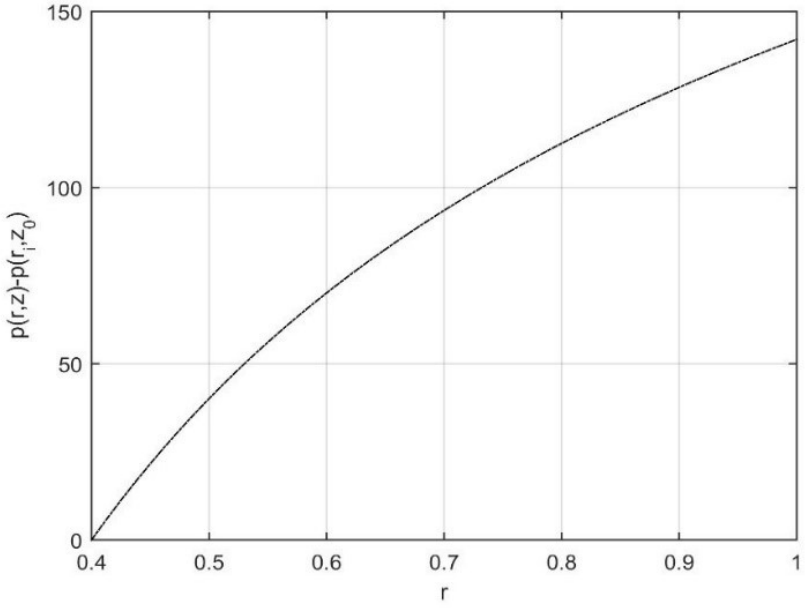

Figure 4.10: Radial distribution of pressure $p(r,z) - p(r_i, z_o)$ corresponding to $c/\nu = 2$ based on Eq. (4.24). Other parameters are $\omega_i = 25\ cycles\ s^{-1}$ and $\omega_o = 5\ cycles\ s^{-1}$.

Although according to the general theory of fluid motion, for rigid body rotation of fluid elements with a velocity component half the vorticity vector is required, but this needs to be accelerated; this shock is expected to assist acceleration. Since the parameter c came into existence due to the radial velocity, a particular value of the radial velocity may be thought responsible for the genesis of dust devils. Barring these anomalies, the pressure distribution along the radius for various values of c/ν is similar to what Pandey and Maurya (2017) observed for the case with zero radial velocity.

A similar situation was reported by Onischenko et al. (2016) in which they pointed out an explosive growth of an unsteady dust devil under the assumption that vorticity is constant with height. This was attributed to the presence of double exponential term in vertical vorticity.

Gradual axial pressure changes are also responsible for the funnel like shape of a whirlwind. Dust devils being short in size take sometimes right circular cylindrical shape. However, in the beginning due to larger compressive pressure in the vicinity of the ground dust devils too look like a funnel.

4.4 Conclusions

The main conclusions of the entire discussion of this article are associated with the inflow parameter c of the radial component of velocity without which no formation of a dust devil can be thought of. The axial velocity reduces smoothly to that derived by Pandey and Maurya (2017) for no radial velocity. The azimuthal component has no discontinuity for $c \to o,\ \nu\ or\ 2\nu$. However, in spite of the fact that $c \to 2\nu$ does not lead to any discontinuity in pressure, it rises enormously at once, almost as an explosion having different limits depending on the radial coordinate, in a very small

neighborhood of $c = 2\nu$. This causes compression and accelerates the formation of dust devils based on conservation of angular momentum. This situation is probably a fluid dynamic root cause, i.e., the driving force for the genesis of dust devils.

Appendices

Appendix A

Let the axial velocity $w(r, z)$ be given by

$$w(r, z) = f(r) \times g(z),$$

where $f(r)$ and $g(z)$ are respectively functions of only r and only z. Substituting this product into Eq. (4.7), we obtain

$$u\frac{df}{dr} = -\frac{1}{\rho g(z)}\frac{\partial p}{\partial z} + \nu\left(\frac{d^2 f}{dr^2} + \frac{1}{r}\frac{df}{dr} + \frac{f}{g(z)}\frac{d^2 g}{dz^2}\right) - f^2\frac{dg}{dz}. \tag{A1}$$

Here the radial velocity u may be solved as a function of r and z; but in view of several solutions in the literature considering u a function of only r (Burgers, 1940, 1948; Long, 1957; Rott, 1958; Tanamachi et al., 2006; Yih, 2007; Makarieva and Gorshkov, 2009*a*, *b*, 2011; Bestray et al., 2011; Makarieva et al., 2011; Arsen'yev, 2011; Bistray and Lykov, 2012; Rotunno, 2013; Davies-Jones, 2015; Ben-Amots, 2016; Baker and Sterling, 2017 etc.) and also for the sake of avoiding complicacies, we consider the radial velocity u a function of only r. Further, following the assumption made by Pandey and Maurya (2017) for the axial pressure gradient, we consider the pressure gradient $\partial p/\partial z$ a constant.

Under the assumption mentioned above, the equation ($A1$) is satisfied if $g(z)$ is constant. As a consequence, the axial velocity is found to be independent of z, i.e., $w(r)$ is a function of only r.

Appendix B

The radial pressure gradient $\partial p/\partial z = P$ which, when integrated with respect to z, gives $p(r, z) = zP + k(r)$, where $k(r)$, being a function of r; yields $k(r) = p(r, z_0) - z_0 P$, when it is evaluated at $z = z_0$. Hence $p(r, z) = p(r, z_0) + P(z - z_0)$.

Appendix C

In the subsection 2.4, P symbolising $\partial p/\partial z$, is constant. Hence, $p = Pz + k(r)$, where $k(r)$ is a function of r. Therefore, $\partial p/\partial r$ is a function of only r. Further, Eq. (4.5) may be rearranged as follows:

$$v^2 = r \times \left\{ u\frac{du}{dr} + \frac{1}{\rho}\frac{\partial p}{\partial r} - \nu\left(\frac{d^2u}{dr^2} + \frac{1}{r}\frac{du}{dr} - \frac{u}{r^2}\right)\right\}. \tag{C1}$$

The right hand side terms involve r and parameters $u(r)$ and $p(r)$, which are functions of only r as per the expression (4.10), and the discussion in this section itself respectively. Therefore, v has to be a function of r and none other.

Appendix D

Since the flow is considered steady, the streamlines and path lines coincide. Streamlines are solutions of $dr/u = rd\theta/r\omega = dz/w$, which give

$$\theta = -\frac{1}{c\left(r_o^{2-c/\nu} - r_i^{2-c/\nu}\right)}\left\{r_i^{2-c/\nu} r_o^{2-c/\nu}\left(\omega_i r_i^{c/\nu} - \omega_o r_o^{c/\nu}\right)\log(r) - \frac{\left(r_i^2\omega_i - r_o^2\omega_o\right)r^{2-c/\nu}}{2-c/\nu}\right\} + const., \tag{D1}$$

and

$$z = -\frac{r^2}{2c}\left[w_o - \frac{g\frac{\rho_\infty - \rho}{\rho_\infty} + P}{c\rho\left(2 + c/\nu\right)}\left\{r_i^{2+c/\nu}\left(r_o^{-c/\nu} - \frac{2r^{-c/\nu}}{2-c/\nu}\right) + \frac{c}{2\nu}\left(r_o^2 - \frac{r^2}{2}\right)\right\}\right] + const., \tag{D2}$$

The two equations reduce respectively to

$$\theta = -\frac{\log(r)\left\{\omega_o r_o^2 \log\left(\frac{r_i^2}{r}\right) - \omega_i r_i^2 \log\left(\frac{r}{r_o^2}\right)\right\}}{2c\log\left(\frac{r_i}{r_o}\right)} + const., \tag{D3}$$

and

$$z = -\frac{1}{2\nu}\left[\frac{r^2}{2}w_o - \frac{g\frac{\rho_\infty - \rho}{\rho_\infty} + P}{8\rho\nu}\left\{r_i^4\left(\frac{r^2}{2}r_o^{-2} - \log(r)\right) + \frac{r^2}{2}\left(r_o^2 - \frac{r^2}{2}\right)\right\}\right] + const. \tag{D4}$$

as $c/\nu \to 2$. The same are the values the function obtained by direct substitution from the beginning showing continuity of the functions at $c = 2\nu$.

****